Investigating Effect of Space Radiation Environment on Piezoelectric Sensors: Cobalt-60 Irradiation Experiment

Mary Anderson
Mem. ASME
Department of Mechanical Engineering,
New Mexico Institute of Mining and Technology,
Socorro, NM 87801
e-mail: Mary.Anderson@student.nmt.edu

Andrei N. Zagrai[1]
Mem. ASME
Department of Mechanical Engineering,
New Mexico Institute of Mining and Technology,
Socorro, NM 87801
e-mail: Andrei.Zagrai@nmt.edu

Joshua D. Daniel
White Sands Missile Range,
Las Cruces, NM 88002
e-mail: Joshua.d.daniel4.civ@mail.mil

David J. Westpfahl
Physics Department,
New Mexico Institute of Mining and Technology,
Socorro, NM 87801
e-mail: David.Westpfahl@nmt.edu

Dale Henneke
Materials Department,
New Mexico Institute of Mining and Technology,
Socorro, NM 87801
e-mail: Dale.Henneke@nmt.edu

Piezoelectric sensors are used in many structural health monitoring (SHM) methods to interrogate the condition of the structure to which the sensors are affixed or embedded. Among SHM methods utilizing thin wafer piezoelectric sensors, embedded ultrasonics is seen as a promising approach to assess condition of space structures. If SHM is to be implemented in space vehicles, it is imperative to determine the effects of the extreme space environment on piezoelectric sensors in order to discern between actual structural damage and environmental effects. The near-Earth space environment comprises extreme temperatures, vacuum, atomic oxygen, microgravity, micrometeoroids and debris, and significant amounts of radiation. Gamma radiation can be used to emulate the space radiation environment. In this contribution, the effects of gamma radiation on piezoelectric ceramic sensors are investigated for equivalent gamma radiation exposure of more than a year on low Earth orbit (LEO). Two experiments were conducted in which cobalt-60 was utilized as the source of radiation. Freely supported piezoelectric sensors were exposed to increasing levels of gamma radiation. Impedance data were collected for the sensors after each radiation exposure. The results show that piezoelectric ceramic material is affected by gamma radiation. Over the course of increasing exposure levels to cobalt-60, the impedance frequencies of the free sensors increased with each absorbed dose. The authors propose that the mechanism causing these impedance changes is due to gamma rays affecting piezoelectric, electric, and elastic constants of the piezoelectric ceramic. A theoretical model describing observed effects is presented.

[DOI: 10.1115/1.4037684]

Keywords: piezoelectric ceramic sensors, gamma radiation, impedance structural health monitoring

1 Introduction

The need to identify and assess damage in space structures has become increasingly important as the commercial space industry develops new generations of space vehicles. The primary goal of integrated structural assessment or structural health monitoring (SHM) is to reduce risk of accidents while minimizing launch and maintenance costs. A broad range of SHM methods has been developed and has demonstrated utility in determining launch readiness of space structures and reusable parts.

After the Columbia shuttle disaster in which the wing of the craft was damaged by foam tile impact, the National Aeronautics and Space Administration began to implement nondestructive evaluation and SHM into the inspection regimen [1]. Inspection methods employed by National Aeronautics and Space Administration include eddy current, X-ray and thermography [2], three-dimensional laser reconstruction [3], as well as imaging techniques [4] for many parts before and after test flights. These methods are used primarily after visual inspections to identify areas of concern or repair. Damage to a launch vehicle or space structure may also occur before assembly, because parts are manufactured, stored, and then shipped to the launch site for assembly. Damage may occur during any of these phases [2], as well as during one of the most critical phases—space vehicle assembly. Inspection during assembly plays a pivotal role in assuring structural integrity and adequate performance. Currently, visual inspection is the dominant method of condition assessment during structural assembly. However, it cannot determine condition of joints and evaluate inaccessible locations. SHM methods have shown promise in detecting loose bolts and inadequate joints [5,6] and supporting a prelaunch diagnostics process which results in "go" or "no go" launch decision. It is envisioned that structural health monitoring could provide information on structural condition during all stages of the space flight, from launch to on-orbit operation to re-entry and recovery. If structural health monitoring is to be used effectively in space structures, then such systems must withstand the effects of the extreme space environment including microgravity, atomic oxygen, extreme temperatures, vacuum, and radiation [7].

Space environment may influence SHM system in a number of ways. Outgassing, metal whiskers, and thermal gradients are just a few examples. This contribution focuses on effects of radiation on sensors as critical elements of SHM system. Among many sensors used in SHM, piezoelectric sensors are, perhaps, the most popular. Although piezoelectric sensors come in different forms, shapes, and assemblies, thin piezoelectric disks or plates, often called piezoelectric wafer active sensors (PWASs), are a typical choice for embedded systems. Such systems have only recently been proposed for SHM of space vehicles [5], and investigation of sensors' performance under typical spaceflight conditions is of considerable interest. It is expected that vacuum and extreme temperatures of space, as space vehicle transits from day to night, influence

---

[1] Corresponding author.

Manuscript received June 5, 2017; final manuscript received August 10, 2017. Editor: Tribikram Kundu.

piezoelectric sensor performance. Temperature effects on piezoelectric sensors were studied for increasingly higher temperatures [8,9] and for increasingly colder temperatures [10]. Influence of temperature on SHM results during a suborbital spaceflight has also been reported [11]. The aim of this contribution is to study radiation effects on piezoelectric sensors and develop a predictive model to account for influence of radiation on piezoelectric sensors operating in extreme environments.

1.1 Radiation in Space. Radiation in the space environment comes from three major sources: solar particle radiation (from within the solar system), galactic cosmic radiation (from outside of the galaxy), and trapped particle radiation (from within the Van Allen Belts). Much data have been compiled on the effect of high-particle radiation as it pertains to crewed missions and shielding. The greatest particle density emanates from the sun in the form of solar wind. Solar events contribute spikes in the particle flux. Protons comprise the bulk of the particle radiation from solar wind and solar events. The next most abundant particles are alpha particles, although heavy nuclei have been observed in the radiation from major solar events. Galactic cosmic radiation comes from beyond our solar system and is mostly fully ionized nuclei which comprise up to a third of the interstellar energy density. These nuclei come from nearly all of the elements including the radioactive actinide group (Z-89 through Z-103) [7]. Radiation energy ranges from kilo-electron-volt for trapped electrons in the Van Allen Belts to giga-electron-volt for galactic cosmic radiation and solar heavy ions [12]. The particles trapped within the Van Allen Belts are protons and electrons. Even within the Van Allen Belts, radiation exposure can fluctuate by orders of magnitude in a magnetic storm [13]. Space structures on low Earth orbit (LEO) will encounter all of these forms of radiation to varying degrees, depending on the period in the solar cycle and on the altitude, inclination, and duration of the orbit.

1.2 Simulating the Space Radiation Environment. Radiation in space is a complex mix of particles as well as secondary effects, making simulation of space radiation a difficult endeavor [14]. Naturally occurring radiation in the solar system ranges in energy from 10 keV (for Van Allen Belts radiation) to over 30 MeV (for a solar event). Depending upon the purpose of the radiation simulation, approximations of space radiation can be adequately achieved. Cobalt-60 is used to simulate ionization effects that occur in space due to radiation and can produce the levels of radiation energy that occur within the Van Allen Belts [14]. Cobalt-60 is an unstable isotope that emits two photons of energy as it returns to relative stability. The first and most abundant emission is approximately 1.173 MeV which comprises about 99% of the photon emissions of cobalt-60. The second emission is approximately 1.332 MeV. High doses of gamma rays emanate from cobalt-60 and can achieve ionization in a few hours that would take years in space. The rate in space for a high-radiation orbit is approximately 0.3 rad/h [15]. Supernovae, pulsars, and neutron stars produce gamma radiation. The European Space Agency states that, "ionization due to gamma rays provides a useful simulation of the penetrating electrons and protons in the space radiation spectrum" [15].

1.3 Radiation Effects on Piezoelectric Ceramic Sensors. The effect of radiation on piezoelectric ceramic sensors is of interest in the development of continuous structural health monitoring methods such as the embedded ultrasonics and the electromechanical impedance method. In the aforementioned methods, piezoelectric sensors are bonded or imbedded in a structure, and a mechanical wave is sent through the material that allows for the inferring of structural dynamic characteristics that, due to the direct piezoelectric effect, are reflected in electromechanical signature of a piezoelectric sensor. If material or structural damage is present, there will be a change in the elastic wave and structural dynamics signatures, and hence, in the impedance measured by piezoelectric sensor [16]. If piezoelectric sensors are considered for operation in radiation environments, then understanding the effects of radiation on piezoelectric ceramics is imperative.

In 1965, Glower et al. investigated radiation on lead-zirconate-titanate (PZT) ceramics in high neutron flux and gamma radiation. The researchers subjected the PZT ceramics to 3×10^{13} neutrons/cm^2 s and 10^9 rad (H_2O)/h. Remanent polarization began to decrease in the piezoelectric material. Polarization hysteresis loop changed from symmetric to asymmetric, then to antiferroelectric-type hysteresis [17]. Fifteen years later, Broomfield demonstrated that irradiation reduces capacitance and electromechanical coupling in PZT ceramics. Increase in resonant frequency was also detected [18]. Meleshko et al. tested different thicknesses of piezoelectric transducers in a reactor where the specimens were exposed to fast neutrons ($E > 1.15$ MeV) and gamma radiation. In these tests, capacitance decreased for all thicknesses, but less so in thicker specimens (4 mm). Resistance decreased for all transducers regardless of thickness [19].

Some research is available on piezoelectric sensors for use in nonvolatile random access memory in an irradiated environment. In 1990, Schwank et al. investigated the effect of radiation on the retained polarization in PZT, as this is an important factor in nonvolatile random access memory. The results showed degradation of the retained polarization in some processes. The exposure to gamma radiation in the range of 225 rad (Si) was enough to cause displacements in the piezoelectric ceramic [20]. The researchers postulate that the radiation-induced damage in the piezoelectric capacitors is due to transport and trapping of electrons, possibly because of defects in the material. A few years later, Moore et al. subjected PZT capacitors to ionizing radiation and found that the retained polarization decreased by 50% [21]. Miclea et al. irradiated lead-zirconate-titanate with neutrons and concluded the decrease in dielectric constants and increase in mechanical quality was due to substitution of ions with higher valences which caused oxygen vacancies in the crystal lattice [22].

Recently, Lin et al. conducted an experiment on the effects of radiation on the PWAS. In this experiment, PWASs were subjected to gamma radiation. After 8 h of exposure, the piezoelectric sensors showed decreased operating temperature, decreased capacitance, and increased resonance frequencies, including the thickness mode [23]. Giurgiutiu et al. analyzed the effects of radiation, temperature, and vacuum on PWAS. The comprehensive experiment describing combined influence of these effects suggested reliability of PWAS under such complex conditions [24].

It is clear from the literature that radiation affects the piezoelectric material used as sensors in a variety of SHM methodologies. Although some piezoelectric materials have been investigated in radiation environment, and selected measurements taken, including the electromechanical impedance measurements, explanation of the mechanisms that cause the changes in impedance frequency of PWAS are not available. The experiments described in this contribution focus on electromechanical response of piezoelectric sensors in an irradiated environment and are aimed at exploring the mechanism behind the radiation-induced changes in the collected dynamic signatures. It is anticipated that the insights gained from the experiments will guide modeling efforts to enable compensation of radiation effects in application of the embedded ultrasonics and the electromechanical impedance method in space and other harsh environments.

2 Experimental Setup and Procedures

The experiments were designed to identify the effects of gamma radiation on the SHM electromechanical impedance method at increasing levels of absorbed dose of gamma radiation. The tests were performed at White Sands Missile Range (WSMR) Gamma Radiation Facility and were designed to emulate radiation exposure of 3 months, 6 months, and 1 year on LEO [25]. The

Table 1 Experimental equipment

Item	Comments
Cobalt-60 (Co-60) gamma irradiation facility	Provided by WSMR
Fluke ion chamber 33cc	Fig. 1 3.2%calibration uncertainty
Fluke Biomedical Advanced Therapy Dosimeter 35040	Calibration due date: July 2016
TLDs	Fig. 2
Kestrel 4000 Weather Tracker	Fig. 1
Cypher Instruments C-60 impedance analyzer with dedicated software	Utilized in the first experiment for collecting sensor J1 data
HP 4192A LF impedance analyzer with National Instruments control software	Utilized in the second experiment for collecting sensors M1 and M2 data

Note: Thermoluminescent dosimeter (TLD).

radiation exposure is expressed in rad (Si)—radiation absorbed dose in silicon.

2.1 Experimental Equipment and Sensors. Equipment utilized in the experiments is listed in Table 1 and includes cobalt-60 radiation source, a variety of environmental sensors and dosimeters, as well as equipment for measuring the electromechanical impedance of the sensors. Photographs of the experimental setup are presented in Fig. 1. The gamma radiation source was movable inside the chamber which allowed for control of the radiation exposure. Levels of radiation were monitored using Fluke ion chamber connected to a dosimeter, Kestrel weather tracker, and TLDs. We are particularly interested in the radiation dose absorbed by the material rather than overall radiation exposure. Materials absorb radiation differently. Absorbed dose is often reported as radiation absorbed dose in silicon (rad (Si)). By utilizing thermoluminescent dosimeters, we can estimate the absorbed dose. Manganese calcium fluoride (Mn:CaF$_2$) is an ideal TLD material for this application, because its response to gamma radiation very closely mirrors that of elemental silicon. The TLD measurement methods at WSMR are traceable from the National Institute of Standards and Technology, but there is an inherent uncertainty of about 8%. The conversion factor enabling conversion from roentgen to rad (Si) was 0.866. Methodology used for TLD testing, processing, and analysis follows all of the guidelines of the American Society of Testing and Materials E666 and E668.

Three lead-zirconate-titanate piezoelectric ceramic sensors investigated in the experiments were manufactured by American Piezo Company (APC, Mackeyville, PA) from APC 851 and APC 850 piezoelectric ceramic materials. As depicted in Figs. 2 and 3, the sensors are piezoelectric disks with top and bottom surfaces covered with silver electrodes. Sensor J1 is APC 851 wrap-around electrode structure allowing for a single side lead connection. The dimensions of the J1 sensors are 6.9558 mm diameter and 0.2527 mm thickness. Sensor M1 is APC 851 with solid silver electrode surfaces on both sides and dimension of 6.9 mm diameter and 0.224 mm thickness. Sensor M2 is APC 850 with solid silver electrode surfaces on both sides and dimensions of 6.35 mm diameter and 0.90 mm thickness. American wire guide 32 leads of 20 cm length were soldered to the sensors using 0.015-diameter, silver bearing solder. During experiments, sensors were suspended in free condition, as illustrated in Fig. 2.

2.2 Experiment Procedures. In the first experiment, the sample plate and free sensor J1 were set inside of a Co-60 gamma irradiation facility on a standard metal testing Table 1 inside of a concrete irradiation cell. Fifty-five feet of serial cable with nine-pin connectors was run from the control room to the samples. In the second experiment, the sample plate and two free sensors (M1

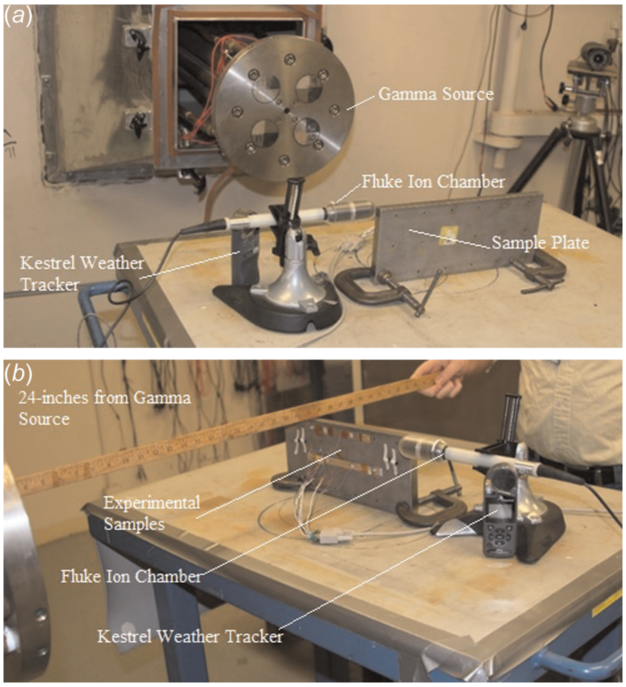

Fig. 1 Experimental setup in the gamma radiation chamber: (*a*) gamma source, testing equipment, and a steel plate with samples and (*b*) front view of plate showing details of the setup, Fluke dosimeter, and Kestrel weather tracker

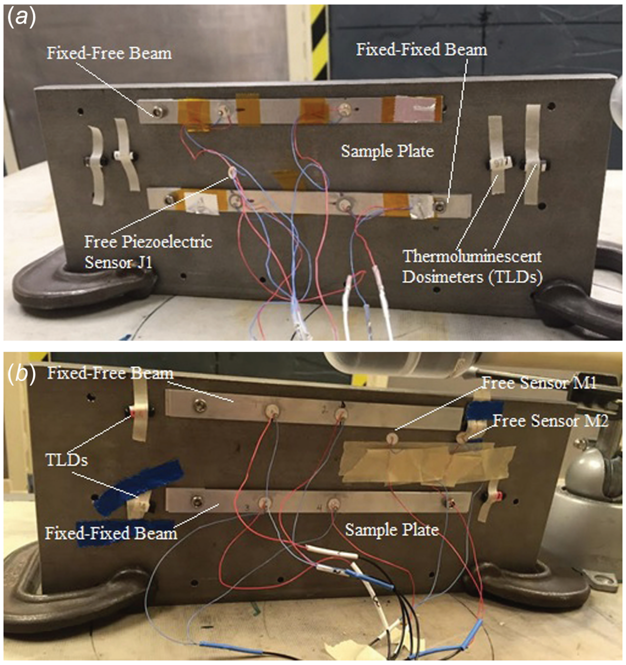

Fig. 2 (*a*) Experimental setup on a steel plate for experiment 1 and (*b*) experimental setup on a steel plate for experiment 2

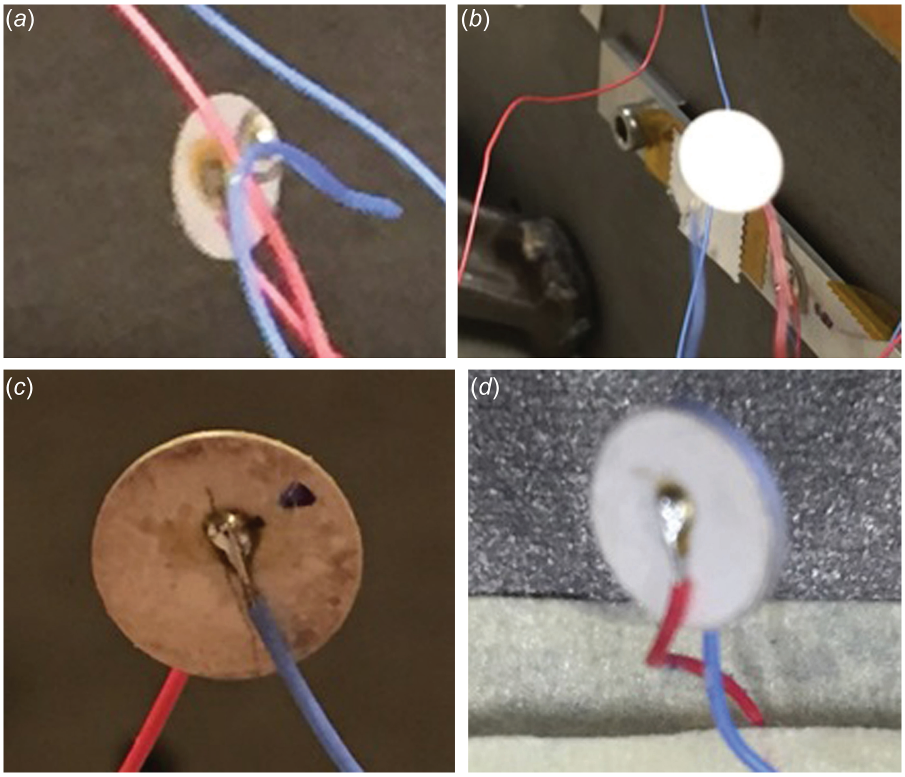

Fig. 3 Photographs of piezoelectric sensors: (*a*) sensor J1 front before irradiation, (*b*) sensor J1 back after 200 krad (Si) exposure, (*c*) sensor M1 after being exposed to 275 krad (Si) dose, and (*d*) sensor M2 after being exposed to 275 krad (Si) dose

and M2) were placed in the gamma radiation chamber on the same stand under the same conditions. However, the impedance readings were taken directly from the sensor connectors in the gamma chamber after each exposure, to avoid cable run from the control room to the chamber.

Mn:CaF_2 TLDs were taped to the steel plate near the samples, as illustrated in Fig. 2. Two TLDs were used for the first irradiation at 10 krad (Si), and four TLDs were used for each irradiation thereafter. The TLDs were collected after each irradiation interval and replaced in the same locations with new TLDs.

Pretests were conducted to ensure that a signal was obtained from each sensor. The frequency range selected was 200–250 kHz for sensor J1. The frequency range selected for sensors M1 and M2 was 300–400 kHz. The impedance magnitude data for sensor J1 were collected using the Cypher Instruments C-60 analyzer in the first experiment. The real and imaginary parts of impedance, along with admittance, susceptance, and phase for both parts, were measured for sensors M1 and M2 using the Hewlett Packard (HP) 4192 A impedance analyzer.

The Fluke ion chamber was placed to the side of the samples at a distance of 24-in from the radiation source to monitor the radiation and communicate to the Fluke dosimeter which was being continually monitored in the control room.

2.2.1 *Irradiation Equilibrium.*

A distance of 24 in from the irradiation source was selected to ensure adequate, uniform coverage of the samples. At this distance, there is minimal exposure gradient on the samples. No shielding was used to negate the down-scattered radiation; therefore, there is lower energy gamma radiation absorbing into the samples, and true equilibrium is not achieved. The down-scattered gamma rays have a negligible effect. The Co-60 gamma radiation peaks of interest at 1166 keV and 1333 keV were achieved and constituted the majority of the gamma rays incident on the samples.

2.2.2 *Cobalt Source Strength and Target Exposure Levels.*

The Co-60 sources were refueled in July of 2012. Each source was approximately 15 kilocuries (kCi) when refueled. An approximate activity of the sources at the time of exposure was calculated using the following equation:

$$A(t) = A_0 \cdot e^{-\lambda t} \tag{1}$$

where λ relates to the half-life, $\tau_{1/2}$

$$\lambda = \frac{\ln(2)}{\tau_{\frac{1}{2}}} \tag{2}$$

The half-life of Co-60 is 5.2714 years (1925.38 days). On the date of irradiation for the first experiment, Jan. 19, 2016, the sources were 1298 days from the initial fueling date. Using these values, calculation results in each source being at approximately 9.4 kCi. All four sources were used during irradiation, making the total activity of the source 37.6 kCi.

Table 2 Target absorbed dose and LEO approximation

Experiment		Target absorbed dose krad (Si)	Low Earth orbit approximation
1	2	10	
1	2	25	
1	2	50	
1	2	75	3 months
1	2	100	
1	2	125	6 months
1	2	150	
1	2	200	12 months
	2	250	
	2	275	

Table 3 Experiment 1: Gamma radiation absorbed dose over the entire sample plate

Target dose (rad (Si))	Target exposure (R)	Actual exposure (R)	Estimated dose (rad (Si))	Actual dose (rad (Si))	% difference	Estimated total absorbed dose (rad (Si))	Actual total absorbed dose (rad (Si))	% difference
10,000	11,547	11,494	9954	—	0.00	9954	9954[a]	0.00
25,000	28,868	16,119	13,959	14,175	1.52	23,913	24,129	0.90
50,000	57,737	31,110	26,941	26,270	−2.56	50,854	50,399	−0.90
75,000	86,605	24,560	21,269	21,335	0.31	72,123	71,734	−0.54
100,000	115,473	33,100	28,665	28,040	−2.23	100,788	99,774	−1.02
125,000	144,342	28,710	24,863	25,370	2.00	125,651	125,144	−0.40
150,000	173,210	27,320	23,659	22,645	−4.48	149,310	147,789	−1.03
200,000	230,947	62,510	54,134	49,170	−10.09	203,443	196,959	−3.29

[a] TLD datum at 10 krad (Si) was not collected. Therefore, the estimated dose was used as the actual dose in calculating the total dose on the setup. It is reasonable to assume that the difference from the TLD reading and the ion chamber at this point would not exceed 3% based on other low exposure measurements.

Table 4 Experiment 2: Gamma radiation absorbed dose over the entire sample plate

Target dose (rad (Si))	Target exposure (R)	Actual exposure (R)	Estimated dose (rad (Si))	Actual dose (rad (Si))	% difference	Estimated total absorbed dose (rad (Si))	Actual total absorbed dose (rad (Si))	% difference
10,000	11,547	11,790	11,031	11,115	0.76	11,031	11,115	0.76
25,000	28,868	20,220	18,918	19,585	3.40	29,949	30,700	2.44
50,000	57,737	26,000	24,326	23,785	−2.28	54,276	54,485	0.38
75,000	86,605	32,000	29,940	30,145	0.68	84,216	84,630	0.49
100,000	115,473	26,260	24,570	25,520	3.72	108,785	110,150	1.24
125,000	144,342	27,330	25,571	26,265	2.64	134,356	136,415	1.51
150,000	173,210	27,380	25,617	25,835	0.84	159,973	162,250	1.40
200,000	230,947	54,340	50,842	47,240	−7.62	210,815	209,490	−0.63
250,000	288,684	60,310	56,428	51,390	−9.80	267,243	260,880	−2.44
280,000	323,326	30,190	28,247	29,145	3.08	295,490	290,025	−1.88

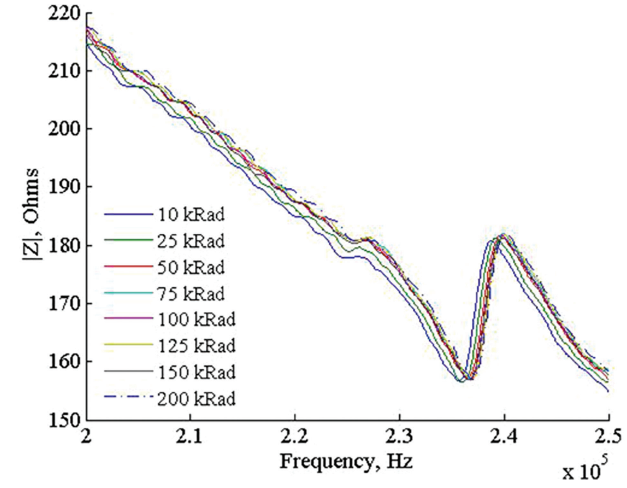

Fig. 4 Impedance magnitude data for sensor J1 at increasing absorbed gamma radiation dose

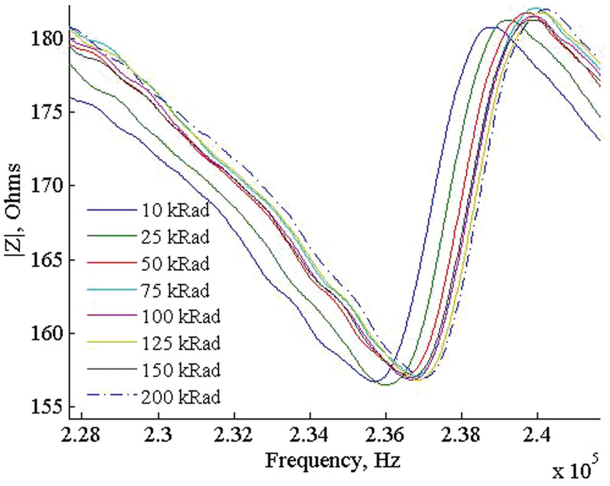

Fig. 5 Sensor J1 enhanced view for the impedance magnitude data at increasing absorbed gamma radiation dose

On the date of irradiation for the second experiment, the sources were 1422 days from the initial fueling date. Therefore, each source was at approximately 8.99 kCi. All four sources were used during irradiation, making the total activity of the source 35.95 kCi.

In order to achieve the target absorbed doses, the samples were irradiated for different time intervals ranging from 9 min to 25 min at an exposure rate of 1283 R/min (1.11 krad (Si)/min). The target total absorbed doses are identified in Table 2.

After each exposure interval, impedance measurements were taken for sensors J1, M1, and M2. The TLDs were retrieved and replaced. The next exposure interval was calculated.

The temperature and atmospheric pressure of the chamber were monitored throughout the experiment. The temperature at the beginning of the first experiment was 16 °C, and the barometric pressure was 26.01 in-Hg. The temperature at the beginning of the second experiment was 27.2 °C, and the barometric pressure was 25.97 in-Hg. These values were used as correction factors for the ion chamber dosimeter.

3 Experimental Results and Discussion

Experiments were conducted for target absorbed radiation doses indicated in Table 2. The details of the target radiation

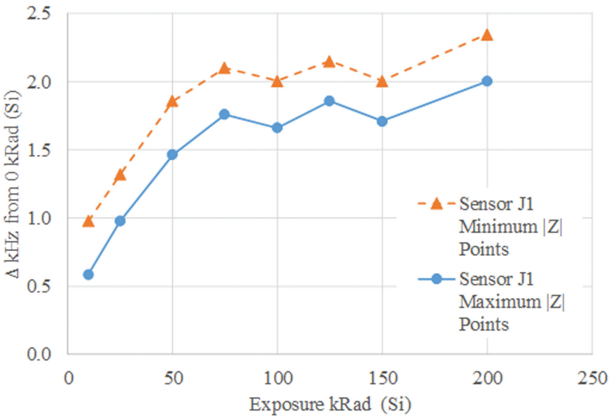

Fig. 6 Sensor J1 plot of |Z| minima and maxima frequencies versus absorbed gamma radiation dose

exposure levels for the first gamma experiment are presented in Table 3, and the target radiation exposure levels for the second gamma radiation experiment are identified in Table 4. In each table, (R) indicates roentgens, and (rad (Si)) indicates radiation absorbed dose equivalent to silicon. The exposure (R), which is approximately (rad (air)), was directly measured by the ion chamber. To calculate estimated dose (rad (Si)), a conversion factor of 0.866 was used. The actual absorbed dose is the dose measured from the TLDs. The light output of the TLD is proportional to the dose received. The dose was estimated using a calibration curve, a fading correction factor (minimal in this batch of sensors), and was averaged in the table for all TLDs that were exposed at each level. For each experiment, the uncertainty did not exceed 10%.

Impedance magnitude signatures were collected at various radiation exposures using Cypher Instruments C-60 impedance analyzer for sensor J1. Experimental impedance curves for this sensor are presented in Fig. 4 with a zoomed-in portion in Fig. 5. It is apparent from the figures that increasing radiation exposure affects sensors impedance in two distinct ways: (a) impedance magnitude across the spectrum increases and (b) frequencies of impedance minima and maxima also increase. Impedance of a piezoelectric sensor is inversely proportional to capacitance, suggesting that capacitance of the piezoelectric sensor decreases as radiation absorbed dose increases. This conclusion is in line with previous experimental observations reporting capacitance decrease under increasing radiation exposure [18,19,23]. It is also evident from the graphs that frequencies of both impedance minima and maxima increase with increase in radiation exposure. Previous studies [18,23] reported increase of resonance frequencies after exposure to radiation. In the present study, frequencies of impedance minima and maxima were extracted from experimental data, and results for the upward frequency shift with respect to frequencies of nonirradiated piezoelectric sensors (0 krad (Si) absorbed dose) are presented in Fig. 6. It can be seen from the figure that frequencies change at higher rate at lower radiation doses, and then the rate of change decreases at higher exposures. In addition, it was observed that as absorption dose increases, frequencies of impedance minima increase more dramatically than frequencies of impedance maxima. Figures 3(*a*) and 3(*b*) provide photographs of sensor J1. According to Fig. 3(*b*), no visible changes in sensor appearance were observed after the sensor was subjected to the maximum 200 krad (Si) exposure. Also shown in Figs. 3(*c*) and 3(*d*) are photos of sensors M1 and M2 after exposure to maximum absorbed dose of 275 krad (Si). Picture of sensor M1 reveals a crack propagating across the sensor. The crack was not a result of radiation exposure, but a damage which likely occurred during transportation of the sensor. The only visible change to sensors due to radiation exposure is darkening of the solder flux at the point of connection with leads. With exception of these observations, there was no visible damage to the piezoelectric sensor after exposure to 275 krad (Si). It should be mentioned that exposure to 275 krad (Si) did not lead to the change of electrode appearance around the edge that was previously observed by Lin et al. [26].

In the second set of experiments, electromechanical impedances of sensors M1 and M2 were collected with the HP 4192A LF impedance analyzer. Broad range impedance plots are presented in Figs. 7 and 8 with details near impedance minima and maxima in Figs. 9 and 10 for sensor M1 and Figs. 11 and 12 for sensor M2. In Fig. 7, the main peak and valley in the impedance curve are not smooth apparently because of a crack in sensor M1. Noticeable in all figures, frequencies of both impedance minima and maxima increase with increase in piezoelectric ceramic absorbed radiation dose. In general, frequency increase is rather continuous with exception of 125 krad (Si) absorbed dose, which seems to be an outlier in the impedance data. No explanation for inconsistency of the impedance reading at this dose is available. As absorption dose increases, frequencies of impedance minima shift further than frequencies of impedance maxima, and the rate of the shift is different. To better understand this effect, resonance and antiresonance frequencies of piezoelectric ceramic sensors M1 and M2 were extracted from impedance phase plots. An

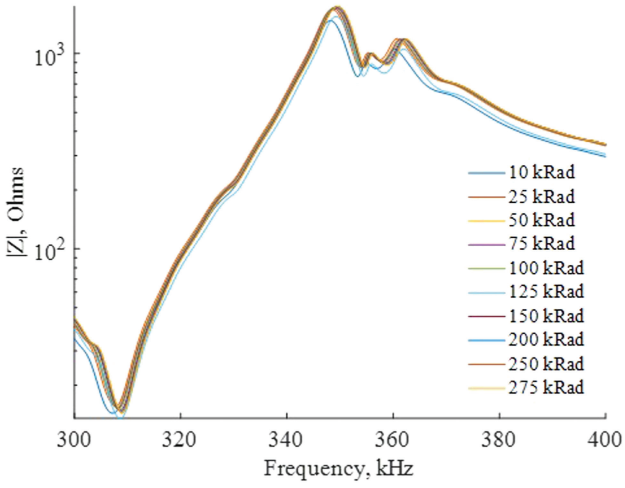

Fig. 7 Impedance magnitude data for sensor M1 at increasing absorbed gamma radiation dose

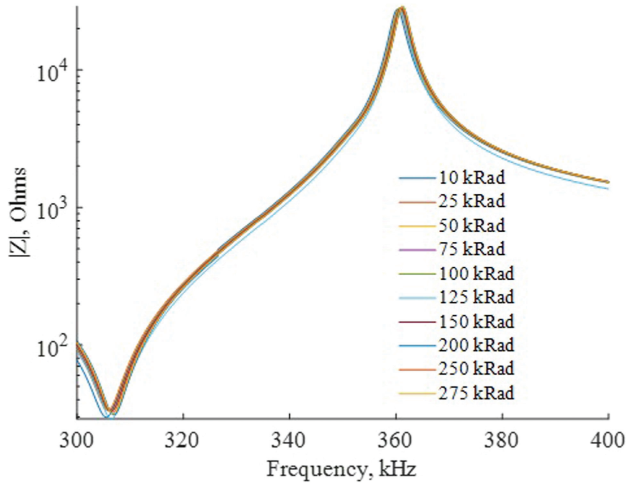

Fig. 8 Impedance magnitude data for sensor M2 at increasing absorbed gamma radiation dose

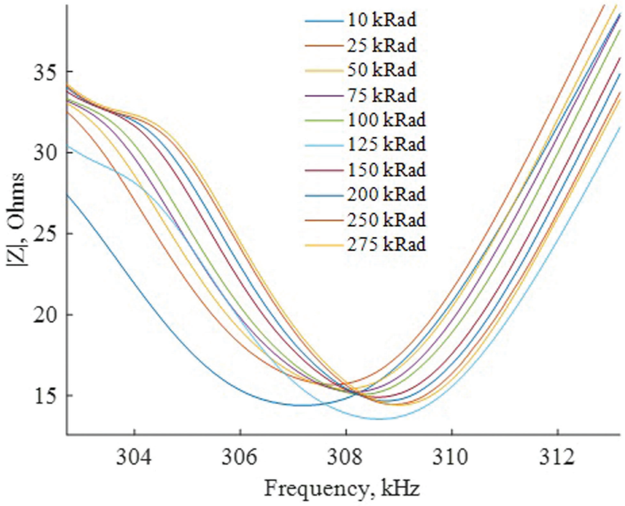

Fig. 9 Enhanced view of impedance minima for sensor M1

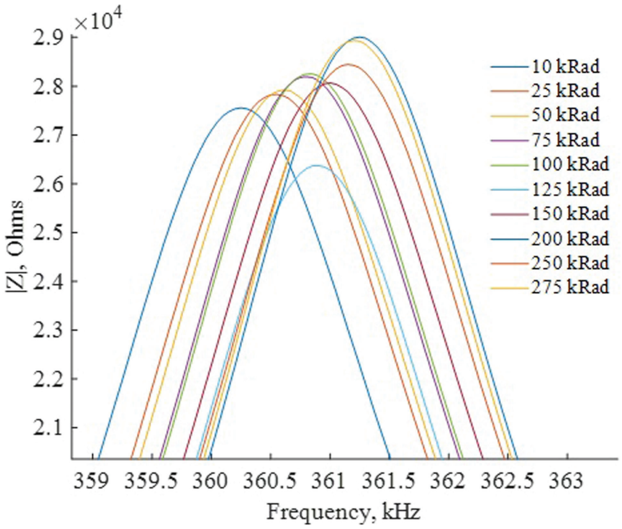

Fig. 12 Enhanced view of impedance maxima for sensor M1

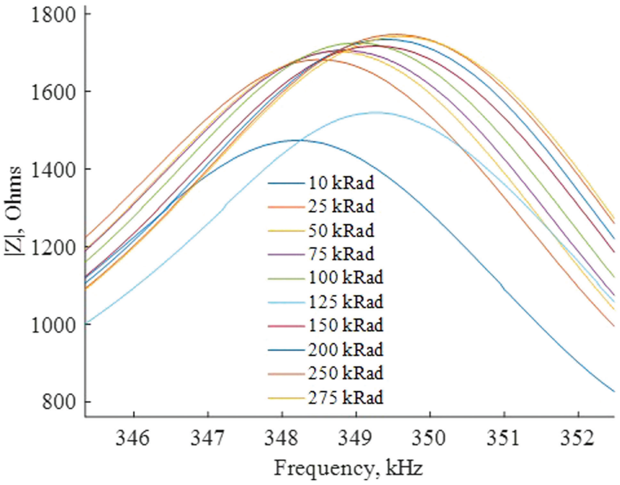

Fig. 10 Enhanced view of impedance maxima for sensor M1

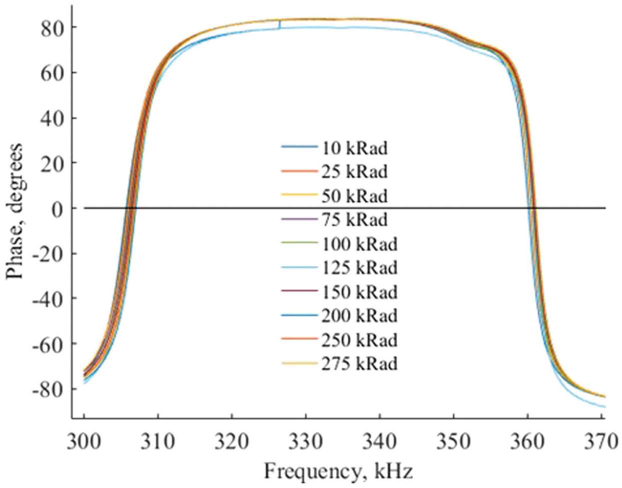

Fig. 13 Impedance phase data for sensor M2 at increasing absorbed gamma radiation dose

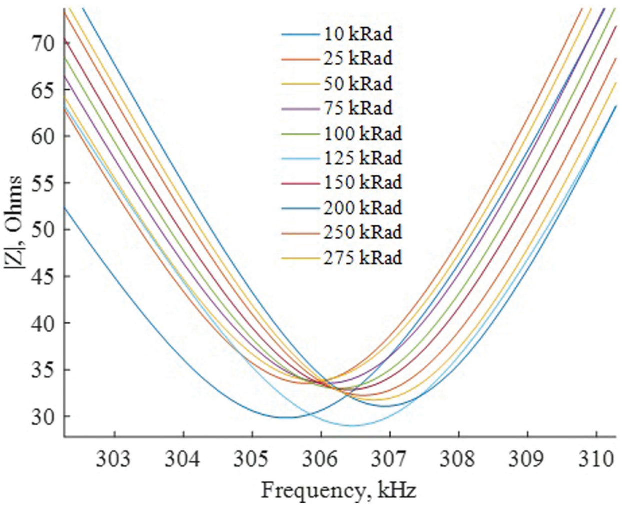

Fig. 11 Enhanced view of impedance minima for sensor M2

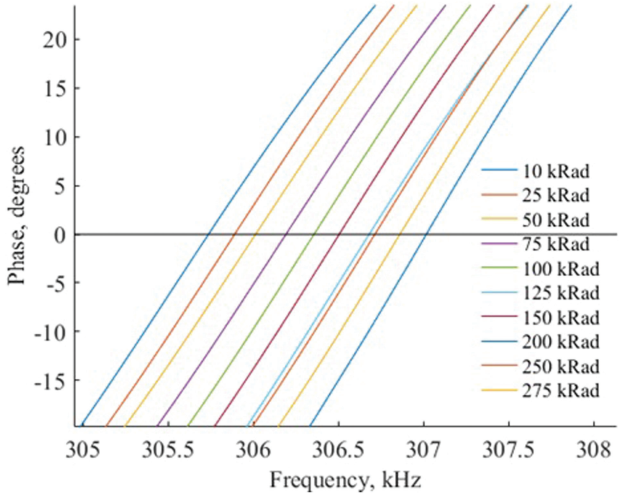

Fig. 14 Enhanced view of the impedance phase near the resonance frequencies of sensor M2

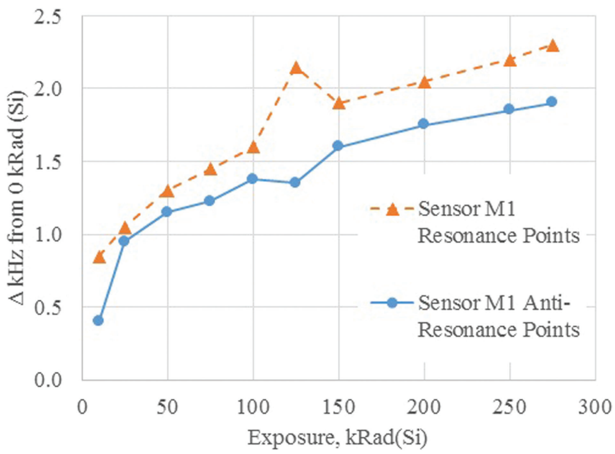

Fig. 15 Sensor M1 plot of resonance and antiresonance frequencies versus absorbed gamma radiation dose

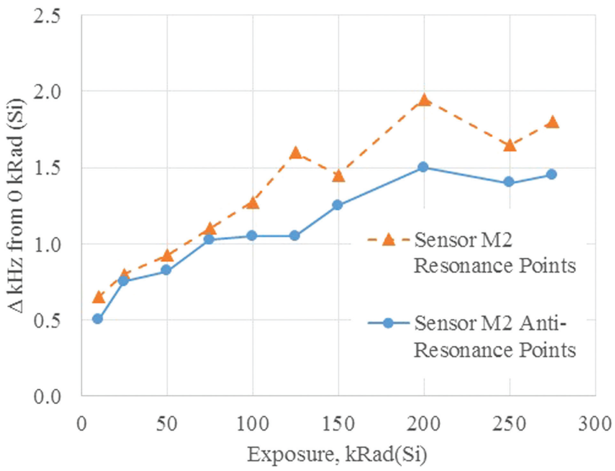

Fig. 16 Sensor M2 plot of resonance and antiresonance frequencies versus absorbed gamma radiation dose

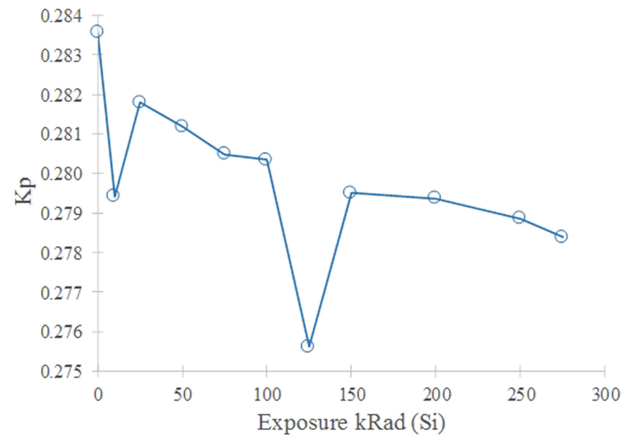

Fig. 17 Planar coupling factor versus absorbed gamma radiation dose for sensor M1

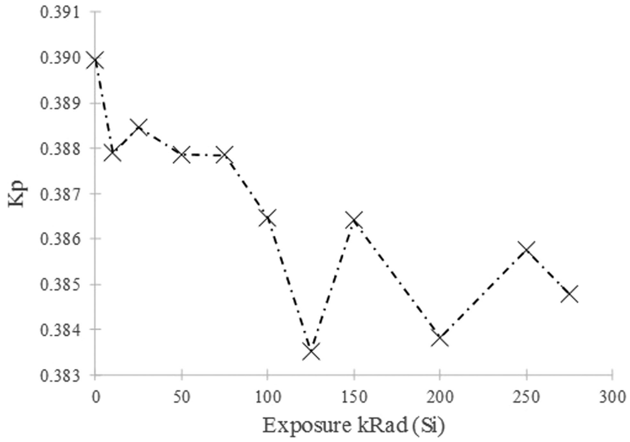

Fig. 18 Planar coupling factor versus absorbed gamma radiation dose for sensor M2

example of impedance phase plot for sensor M2 is presented in Fig. 13. Resonance frequencies were obtained at the points where phase, passing from −90 deg to 90 deg, transitioned the 0-deg line as illustrated in Fig. 14. Antiresonance frequencies were found in a similar way at the points where phase, passing from 90 deg to −90 deg, crossed the 0-deg line. The resultant variations of resonance and antiresonance frequencies versus absorbed radiation dose are presented in Fig. 15 for sensor M1 and in Fig. 16 for sensor M2. The figures suggest that the resonant frequencies are changing faster than the antiresonant frequencies.

An upward impedance frequency shift due to absorbed radiation dose raises a question about which parameters of piezoelectric ceramic control the observed frequency changes. Increase in frequencies may be caused by reduction of material's density or stiffening of the piezoelectric ceramic. Although decrease of density of the piezoelectric ceramic may potentially result in the increase of impedance frequencies, it is unlikely that reported gamma radiation doses noticeably changed material density.

One approach to investigate effect of various parameters of the piezoelectric ceramic on vibration frequencies is to consider the planar coupling factor. According to Ikeda [27], the planar coupling factor depends on piezoelectric, d_{31}, dielectric, ε_{33}^T, and elastic, s_{11}^E, constants of piezoelectric ceramic and is expressed as

$$k_p = \sqrt{2d_{31}^2/[s_{11}^E \cdot (1-\sigma)\varepsilon_{33}^T]} \tag{3}$$

where σ is the Poisson ratio. Resonance and antiresonance frequencies can be used to calculate the planar coupling factor from experimental data in accordance with approximation [28]

$$k_p \approx (f_a^2 - f_r^2)/(f_r^2) \tag{4}$$

Results of calculations for sensors M1 and M2 are presented in Figs. 17 and 18. Numerical values of the planar coupling factor in Fig. 17 are relatively low likely because of the effect of crack on the electromechanical coupling in sensor M1. It is apparent from the figures that although irregularly, planar coupling factor decreases as radiation exposure increases. This observation is consistent with the report by Broomfield [18]. Decrease of the planar coupling under successive radiation exposures makes parameters appearing in Eq. (3), to be primary candidates for consideration in modeling effects of radiation in piezoelectric ceramic.

An additional note needs to be given about capacitance of piezoelectric sensors. Many authors (e.g., Refs. [18,19,21,22], and [26]) reported decrease of capacitance under increased radiation exposures. All sensors in this study demonstrated increase of impedance across measured bandwidths. Given that admittance of the piezoelectric sensor is dominated by capacitance, increase of impedance implies that capacitance of the sensors decreased after sensors were exposed to successive radiation doses. It is

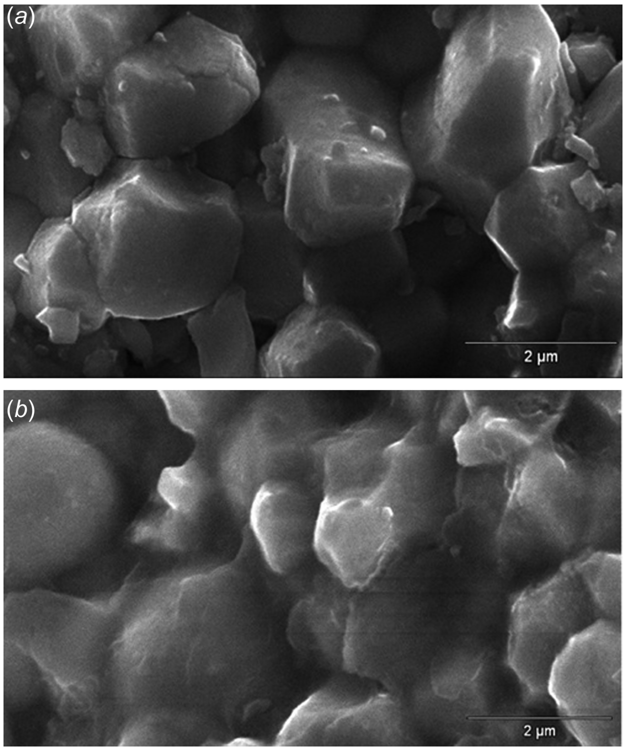

Fig. 19 Scanning electron microscopy (SEM) images of piezoelectric sensor: (*a*) sensor before irradiation and (*b*) M1 sensor after maximum exposure

useful to consider parameters that may be contributing to the decrease of sensor capacitance. For in-plane radial vibrations of piezoelectric disk, the expression for capacitance is [27]

$$C_0 = \varepsilon_{33}^{T} \cdot (1 - k_p^2) \cdot \pi a^2 / t \tag{5}$$

where a and t are radius and thickness of a piezoelectric disk. Analysis of this expression suggests that, in the absence of geometrical changes, a dominant contribution of radiation effects is expected to be reflected in the dielectric permittivity, ε_{33}^{T}.

To explore effect of radiation on the state of piezoelectric material, a sample sensor was subjected to SEM. Piezoelectric material was taken from the part of the piezoelectric sensor where electrodes were absent and a standard procedure for preparation of samples for SEM was followed. Microscopy images of intact (not radiated—0 krad (Si)) piezoelectric sensor and a sensor subjected to maximum dose of 275 krad (Si) are presented in Fig. 19. Damage to the material caused by radiation is clearly visible in Fig. 19(*b*). Grains in the piezoelectric material became less distinct and lost sharp edges. Material generally exhibited "melted" appearance. The observed changes highly likely affected key parameters of piezoelectric material including elastic, piezoelectric, and dielectric constants.

4 Electromechanical Impedance Model Accounting for Effect of Gamma Radiation

Experimental studies demonstrated that subsequent increase of absorbed radiation dose leads to reduction of the planar coupling factor and reduction of sensor capacitance. Equations (3) and (5) detail material constants contributing to reduction of these sensor parameters. An electromechanical impedance model of the sensor is suggested, in which effect of radiation is accounted for using progressive changes of piezoelectric, dielectric, and elastic constants of the piezoelectric ceramic. In-plane radial vibrations of the piezoelectric disk are considered to describe dynamics of the sensor observed in radiation experiments. A classical expression for admittance of a freely suspended, thin, through thickness polarized, piezoelectric disk undergoing radial vibrations is [27,29]

$$Y(\omega) = j\omega C_0 \cdot \left[1 + \frac{k_p^2}{1 - k_p^2} \cdot \frac{(1+\sigma) \cdot J_1(\varphi_d)}{\varphi_d \cdot J_0(\varphi_d) - (1-\sigma) \cdot J_1(\varphi_d)}\right] \tag{6}$$

where J_0 and J_1 are Bessel functions. Argument of the Bessel functions $\varphi_d = \omega a / v$ includes excitation frequency ω, radius of the sensor a, and speed of sound $v = [\rho s_{11}^{E}(1 - \sigma^2)]^{-1/2}$ controlled by elastic compliance s_{11}^{E}, Poisson ratio σ, and density ρ of the piezoelectric ceramic. Poisson ratio $\sigma = -s_{12}^{E} / s_{11}^{E}$ is defined as a ratio of elastic compliances. Inverse of admittance in Eq. (6) is electromechanical impedance $\mathrm{Z}(\omega) = \mathrm{Y}(\omega)^{-1}$.

A theoretical model utilizes Eq. (6) which contains geometrical dimensions of the sensor and its piezoelectric, dielectric, and elastic constants. Electromechanical impedance of sensors not subjected to radiation (0 krad (Si)) was calculated first. Sensors M1 and M2 were fabricated from piezoelectric ceramic APC 851 and APC 850, respectively. Parameters of these piezoelectric ceramics are available from the manufacturer and are included in the model. According to the manufacturer, deviation of parameters by ±20% is possible, and this possibility was accounted for when tuning the model to best match experimental data. Parameters considered in the model are presented in Table 5.

Degradation of the planar coupling factor under increasing radiation exposure suggests that effect of radiation on piezoelectric sensors could be modeled by associated changes in piezoelectric, dielectric, and elastic constants of the piezoelectric ceramic. Variation of each of these constants and their individual influences on resonance and antiresonance frequencies of the sensor were considered, and it was found that changes of only one constant did not adequately model effect of radiation on the piezoelectric sensor. Decrease of material density in the model closely imitated impedances measured for increasing radiation exposures, but, according to Eq. (3), density does not affect the planar coupling factor and levels of gamma radiation utilized in the experiments unlikely caused noticeable changes of material density. For this reason, cumulative changes of piezoelectric, dielectric, and elastic constants, supported by experimentally observed deterioration of the planar coupling factor, were considered as an explanation of the effect of radiation on piezoelectric ceramic sensors.

Table 5 Parameters of PWAS

Parameter	M1 APC 851	M2 APC 850
Thickness (mm)	0.224	0.9
Diameter (mm)	6.9	6.35
Density (kg/m^3)	7.525×10^3	7.5×10^3
Elastic compliance s_{11}^{E} (m^2/N)	$1.495 \times 10^{-11} \times$ (1-1i·0.008)	$1.73 \times 10^{-11} \times$ (1-1i·0.008)
Dielectric permittivity ε_{33}^{T} (F/m)	$1.909 \times 10^{-8} \times$ (1-1i·0.016)	$2.016 \times 10^{-8} \times$ (1-1i·0.016)
Piezoelectric constant d_{31} (C/N)	$-1.67 \times 10^{-10} \times$ (1-1i·0.01)	$-2.10 \times 10^{-10} \times$ (1-1i·0.01)
Poisson ratio σ	0.353	0.331

Note: Imaginary part is signified by 1i.

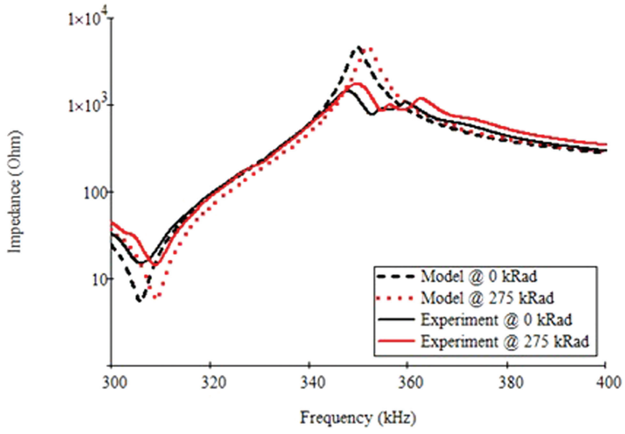

Fig. 20 Experimental and theoretical impedances of sensor M1 exposed to 0 krad (Si) and 275 krad (Si) gamma radiation dose

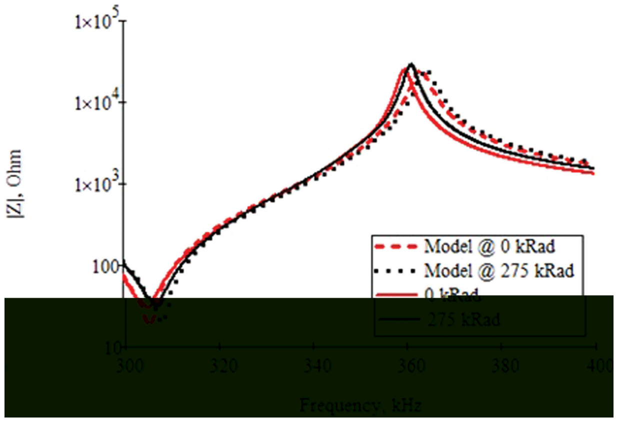

Fig. 21 Experimental and theoretical impedances of sensor M2 exposed to 0 krad (Si) and 275 krad (Si) gamma radiation dose

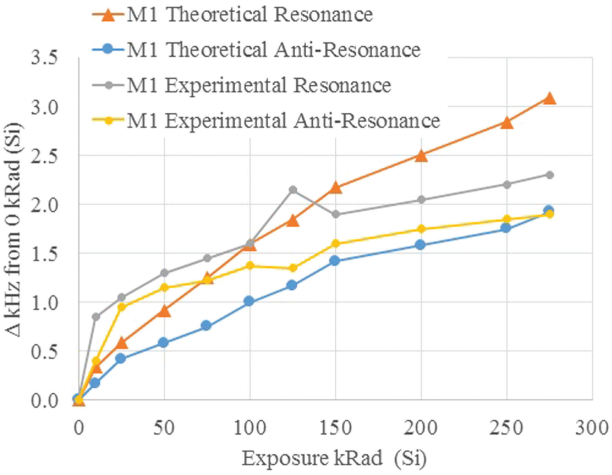

Fig. 22 Experimental and theoretical model data for changes in resonant and antiresonant frequencies of sensor M1 subjected to incrementally increasing radiation exposure

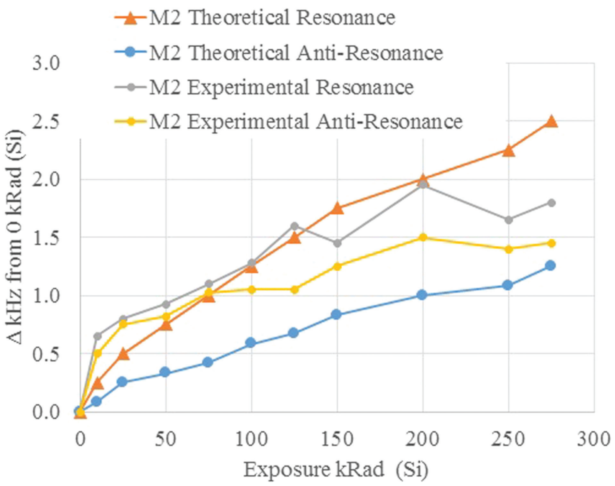

Fig. 23 Experimental and theoretical model data for changes in resonant and antiresonant frequencies of sensor M2 subjected to incrementally increasing radiation exposure

Parameters of the piezoelectric sensors were modeled as follows:

$$
\begin{aligned}
s_{11}^{E*}(i) &= s_{11}^{E*} - (i-1)\cdot \delta s \cdot s_{11}^{E*} \\
\varepsilon_{33}^{T*}(i) &= \varepsilon_{33}^{T*} - (i-1)\cdot \delta\varepsilon \cdot \varepsilon_{33}^{T*} \\
d_{31}^{*}(i) &= d_{31}^{*} - (i-1)\cdot \delta d \cdot d_{31}^{*}
\end{aligned}
\tag{7}
$$

where $i = 1,\ 2,\ldots 11$ corresponds to each subsequent radiation exposure ($i = 1$ for 0 krad (Si)). Incremental changes for APC 850 ceramic were $\delta s = 0.0016$, $\delta\varepsilon = 0.004$, and $\delta d = 0.004$. For APC 851 ceramic, incremental changes were $\delta s = 0.002$, $\delta\varepsilon = 0.003$, and $\delta d = 0.004$. Changes of the Poisson coefficient due to possible anisotropy of radiation effects were estimated to be very small and neglected in the model. The model proposes that radiation primarily affects piezoelectric and dielectric properties of the piezoelectric ceramic and, to the lesser extent, elastic properties.

Theoretical model is compared to experimental data in Figs. 20 and 21. For clarity of presentation, only limited cases of no exposure and maximum exposure were selected. It could be seen that rather good agreement between experimental and theoretical curves was achieved. Details of the progressive changes of resonance and antiresonance frequencies for the range of radiation exposures in practical experiments are presented in Figs. 22 and 23. In the figures, experimental data are superimposed with the data obtained from modeled impedance curves. The plots reveal that theoretical frequencies exhibit wider range of variation, probably due to uncertainty of material parameters used in modeling. In general, theoretical and experimental variations of resonance and antiresonance frequencies are comparable, and it is suggested that the model can be used to predict dynamics of piezoelectric sensor subjected to radiation.

5 Conclusion

Experiments involving Co-60 irradiation of piezoelectric sensors demonstrated ability of the sensors to operate in LEO for extended periods of time. Radiation exposure resulted in an upward shift of resonance and antiresonance frequencies of piezoelectric sensors as well as increase of sensor impedance. The latter is associated with decrease of capacitance, which was also reported by other authors.

In this contribution, reduction of sensor capacitance was modeled by reduction of dielectric permittivity due to radiation.

Consistent with the previous study by Broomfield [18], analysis of resonance and antiresonance frequency shifts under increasing levels of gamma radiation revealed reduction of the planar coupling factor. It was proposed that parameters of the piezoelectric ceramic controlling the planar coupling factor can be used to model effect of radiation in the piezoelectric sensor. A cumulative change of piezoelectric, dielectric, and elastic constants resulted in the theoretical model closely matching experimental data. The change in resonant frequency is caused by the radiation-induced stiffening of the material, which is modeled by reducing elastic compliance. The increase in antiresonance frequency is modeled by decreasing the piezoelectric coefficient. The proposed model utilizes linear variation of piezoelectric, dielectric, and elastic constants, although the experimental data show nonlinear variation at low exposures. Including such a nonlinear dependency in the electromechanical impedance model accounting for radiation effects is a subject of future work. The effects of radiation on the sensor electrode and the solder were not investigated in this experiment and could be the subject of future work.

Acknowledgment

The authors would like to acknowledge Dr. Nickolas Demidovich for guidelines in this research. In addition, the authors acknowledge the following individuals for their invaluable contribution to reported experimental efforts: Josh Blundell, Installation Safety Office, Health Physicists, WSMR; Jerame Lopez, Gamma Range Facility Operator, WSMR; Ricardo Ortiz, Gamma Range Facility Specialist/Operator, WSMR; and Gary Chandler and Nikolai Kalugin, Materials and Metallurgical Engineering Department, New Mexico Institute of Mining and Technology.

Funding Data

- Federal Aviation Administration (FAA) through Center of Excellence for Commercial Space Transportation (COE CST).
- New Mexico Space Grant Consortium.

References

[1] Richards, W. L., Madaras, E., Prosser, W. H., and Studor, G., 2013, "NASA Applications of Structural Health Monitoring Technology," Ninth International Workshop on Structural Health Monitoring, Palo Alto, CA, Sept. 10–12, Paper No. DFRC-E-DAA-TN11102.

[2] Yoder, T. B., and Greene, N., 2010, "Inspection for Damage to Carbon/Epoxy Composite Overwrapped Pressure Vessels," NASA Johnson Space Center, Houston, TX, Technical Report No. JSC-CN-24028.

[3] O'Dell, K. P., 2001, "Automated Inspection of the RSRM O-Ring Seal Surface," AIAA Paper No. 2001-3278.

[4] Nurge, M., Youngquist, R., and Dyer, D., 2013, "Surface Inspection Tool for Optical Detection of Surface Defects," NASA Kennedy Space Center, Cocoa Beach, FL, Technical Report No. KSC-13580.

[5] Arritt, B. J., Robertson, L. M., Williams, A. D., Henderson, B. K., Buckley, S. J., Ganley, J. M., Welsh, J. S., Ouyang, L., Beard, S., Clayton, E. H., Todd, M. D., Doyle, D., and Zagrai, A., 2008, "Structural Health Monitoring: An Enabler for Responsive Satellites," AIAA Paper No. 2008-2166.

[6] Doyle, D., Zagrai, A. N., Arritt, B., and Cakan, H., 2010, "Damage Detection in Bolted Space Structures," J. Intell. Mater. Syst. Struct., **21**(3), pp. 251–264.

[7] Musgrave, G., Larsen, A., and Sgobba, T., 2009, *Safety Design for Space Systems*, Elsevier, Oxford, UK.

[8] Park, G., Kabeya, K., Cudney, H. H., and Inman, D. J., 1999, "Impedance-Based Structural Health Monitoring for Temperature Varying Applications," Jpn. Soc. Mech. Eng., **42**(2), pp. 249–258.

[9] Roy, S., Lonkar, K., Janapati, V., and Chang, F.-K., 2014, "A Novel Physics-Based Temperature Compensation Model for Structural Health Monitoring Using Ultrasonic Guided Waves," Struct. Health Monit., **13**(3), pp. 321–342.

[10] Anderson, M. L., Zagrai, A. N., Doyle, D., Hengeveld, D., and Wilson, M. R., 2015, "Consideration of Thermal Effects in Electro-Mechanical Impedance Measurement for Space Structures," Tenth International Workshop on Structural Health Monitoring (IWSHM), Stanford, CA, Sept. 1–3, pp. 2867–2874.

[11] Zagrai, A. N., Demidovich, N., Cooper, B., Schlavin, J., White, C., Kessler, S., MacGillivray, J., Chesebrough, S., Magnusion, L., Puckett, L., Tena, K., Gutierrez, J., Trujillo, B., Siler, D., and Gonzales, T., 2015, "Structural Health Monitoring During Suborbital Spaceflight," 66th International Astronautical Congress, Jerusalem, Israel, Oct. 12–16, Paper No. C2,5,3,x29660.

[12] Sajid, M., Chechenin, N. G., Torres, F. S., Khan, E. U., and Agha, S., 2015, "Space Radiation Environment Prediction for VLSI Microelectronics Devices Onboard a LEO Satellite Using OMERE-TRAD Software," Adv. Space Res., **56**(2), pp. 314–324.

[13] O'Brien, T. P., Masur, J. E., Guild, T. B., and Looper, M. D., 2015, "Using Polar-Orbiting Environmental Satellite Data to Specify the Radiation Environment Up to 1200 km Altitude," Space Weather, **13**(8), pp. 434–445.

[14] Price, W. E., 1965, "The Simulation of Space Radiation Damage to Spacecraft Systems," IEEE Trans. Nucl. Sci., **12**(6), pp. 2–7.

[15] ESA, 1993, "European Space Agency: The Radiation Design Handbook," ESA Publications Division, Noordwijk, The Netherlands.

[16] Zagrai, A. N., and Giurgiutiu, V., 2009, "Electromechanical Impedance Modeling," *Encyclopedia of Structural Health Monitoring*, Wiley, Chichester, UK.

[17] Glower, D. D., Hester, D. L., and Warnke, D. F., 1965, "Effects of Radiation-Induced Damage Centers in Lead Zirconate Titanate Ceramics," J. Am. Ceram. Soc., **48**(8), pp. 417–421.

[18] Broomfield, G. H., 1980, "The Effect of Low-Fluence Neutron Irradiation on Silver-Electroded Lead-Zirconate-Titanate Piezoelectric Ceramics," J. Nucl. Mater., **91**(1), pp. 23–34.

[19] Meleshko, Y. P., Karpechko, S. G., Leont'ev, G. K., Nalivaev, V. I., Nikiforov, A. D., and Smirnov, V. M., 1985, "Radiation Resistance of the Piezoelectric Ceramics TsTS-21 and TNV-1," At. Energ., **61**(1), pp. 561–564.

[20] Schwank, J. R., Nasby, R. D., Miller, S. L., Rodgers, M. S., and Dressendorfer, P. V., 1990, "Total-Dose Radiation-Induced Degradation of Thin Film Ferroelectric Capacitors," IEEE Trans. Nucl. Sci., **37**(6), pp. 1703–1712.

[21] Moore, R. A., Benedetto, J., and Rod, B. J., 1993, "Total Dose Effect on Ferroelectric PZT Capacitors Used as Non-Volatile Storage Elements," IEEE Trans. Nucl. Sci., **40**(6), pp. 1591–1596.

[22] Miclea, C., Tanasoiu, C., Miclea, C. F., Spanulescu, I., and Cioangher, M., 2005, "Effect of Neutron Irradiation on Some Piezoelectric Properties of PZT Type Ceramics," J. Phys. IV, **128**, pp. 115–120.

[23] Lin, B., Gresil, M., Giurgiutiu, V., Knight, T., Mendez-Torres, A. E., and Yu, L., 2014, "Nuclear Environmental Effects on Piezoelectric Wafer Active Sensors Based Acousto-Ultrasonic Sensing System," International Congress on Advances in Nuclear Power Plants (ICAPP), Charlotte, NC, Apr. 6–9, Paper No. 14304.

[24] Giurgiutiu, V., Postolache, C., and Tudose, M., 2016, "Radiation, Temperature, and Vacuum Effects on Piezoelectric Wafer Active Sensors," Smart Struct. Syst., **25**, p. 035024.

[25] Howard, J. W., Jr., and Hardage, D. M., 1999, "Space Environments Interactions: Space Radiation and Its Effects on Electronic Systems," Marshall Space Flight Center, National Aeronautics and Space Administration, Huntsville, AL, Technical Report No. NASA/TP-1999-209373.

[26] Lin, B., Gresil, M., Giurgiutiu, V., and Mendez-Torres, A. E., 2012, "Structural Health Monitoring With Piezoelectric Wafer Active Sensors Exposed to Irradiation Effects," ASME Paper No. PVP2012-78848.

[27] Ikeda, T., 1996, *Fundamentals of Piezoelectricity*, Oxford University Press, Oxford, UK.

[28] Jordan, T. L., and Ounaies, Z., 2001, "Piezoelectric Ceramics Characterization," NASA Langley Research Center, Hampton, VA, Technical Report No. NASA/CR-2001-211225.

[29] ANSI/IEEE, 1987, "IEEE Standard on Piezoelectricity," IEEE, New York, ANSI/IEEE Standard No. 176-1987.